GEOPHYSICS

The precursory phase of large earthquakes

Quentin Bletery[1]* and Jean-Mathieu Nocquet[1,2]

The existence of an observable precursory phase of slip on the fault before large earthquakes has been debated for decades. Although observations preceding several large earthquakes have been proposed as possible indicators of precursory slip, these observations do not directly precede earthquakes, are not seen before most events, and are also commonly observed without being followed by earthquakes. We conducted a global search for short-term precursory slip in GPS data. We summed the displacements measured by 3026 high-rate GPS time series—projected onto the directions expected from precursory slip at the hypocenter—during 48 hours before 90 (moment magnitude ≥7) earthquakes. Our approach reveals a ≈2-hour-long exponential acceleration of slip before the ruptures, suggesting that large earthquakes start with a precursory phase of slip, which improvements in measurement precision and density could more effectively detect and possibly monitor.

Detecting precursors to natural disasters is key for predicting those events and minimizing human and economic losses. The search for earthquake precursors has been a long-standing pursuit, with much hope being placed in the concept of earthquake prediction in the early 1970s (*1*). The potential for earthquake prediction was later seriously reassessed when theoretical studies suggested that earthquakes are nonlinear processes that are highly sensitive to unmeasurably fine details of the physical conditions at depth (*2*, *3*). In the past decade, the idea has grown that large earthquakes initiate with a potentially observable slow aseismic phase of slip on the fault, associated with increased microseismicity (*4*–*18*). On the basis of either geodetic or seismic data, these studies suggest that earthquake precursors exist and that therefore earthquakes could be anticipated minutes (*4*), days (*5*, *7*, *15*, *18*), weeks (*6*), months (*7*–*12*), or even years (*13*) before they occur.

Nevertheless, all these analyses are based on records preceding only a few earthquakes, strongly limiting the generalization of the observation. Moreover, slow aseismic slip events associated with increased microseismicity are routinely observed and most of the time do not precede a large earthquake (*19*–*24*), which further calls into question the causal relationship between these proposed precursory signals and the earthquakes. Another critical point is that these observations on natural faults do not show a continuous process culminating in the earthquake. Indeed, whether the observations come from geodetic or seismic data, they show evidence of a slow slip or a microseismic crisis that usually stops days or weeks before the catastrophic event (*4*–*6*, *8*–*18*). None of these observations show an exponential buildup of the aseismic slip leading to the rupture, which is expected from laboratory experiments (*25*–*28*) and numerical models (*29*–*31*). One exception is a global analysis of the seismicity preceding large earthquakes, which does find an exponential increase in the number of earthquakes ranging from years up to hours preceding large events (*7*).

Global stack of high-rate GPS data preceding large earthquakes

We investigated the existence of precursory signals in high-rate (5-min) GPS data recorded in the 48 hours preceding moment magnitude (M_w) ≥ 7.0 earthquakes worldwide (Fig. 1). We quantitatively test the hypothesis that earthquakes start with a precursory phase of slow aseismic slip at the location of the hypocenter of the forthcoming event. We calculate the expected displacements measured by GPS stations induced by such precursory slip (*32*). For each earthquake, i, for each station, j, and at each time step, t, we then calculate the dot product of the observed horizontal displacement, $u_{i,j}(t)$, with the horizontal displacement, $\overrightarrow{g_{i,j}}$, expected from a unit precursory slip in the direction of the impending earthquake. If the observation is consistent with precursory slip—that is, if $\overrightarrow{u_{i,j}}(t)$ and $\overrightarrow{g_{i,j}}$ have similar orientations—then the dot product will be positive. If GPS data do not contain any signal related to precursory slip, the dot product, $\overrightarrow{u_{i,j}}(t) \cdot \overrightarrow{g_{i,j}}$, is equally likely to be positive or negative.

Using the global catalog of GPS data processed by the Nevada Geodetic Laboratory (*33*), we calculate this dot product for each earthqake and for each station and then sum their contributions at each (5-min) time step (with respect to the earthquake origin times) to obtain the stack time series

$$S(t) = \sum_{i=1}^{N_{eq}} \sum_{j=1}^{N_{st}(i)} \frac{\overrightarrow{u_{i,j}}(t) \cdot \overrightarrow{g_{i,j}}}{\sigma_{i,j}^2} \quad (1)$$

in the 2 days preceding the earthquake or[illegible] times, where $\sigma_{i,j}$ is an estimate of the n[illegible] amplitude at each station (*32*). Division by the square of the noise amplitude provides a weighted stack (*34*–*36*). The dot product with the expected displacement field, $\overrightarrow{g_{i,j}}$, gives a greater weight to measurements at stations where larger displacement is expected from precursory slip—that is, at stations located close to the hypocenter of the upcoming earthquake. If GPS data do not contain any earthquake precursory signal, we expect S to exhibit no obvious trend. Coherent noise structures reminiscent of colored noise in GPS data are expected to be strongly attenuated by the stack on multiple earthquakes, which should not share coherent noise patterns. Consistently, the distribution of S as a function of time shows no obvious coherent pattern from 48 to 2 hours before the earthquakes (Fig. 2A). However, in the 2 hours preceding the events, the stack reveals a positive trend, supporting the hypothesis of a growing slip in the hypocenter area (Fig. 2A).

Statistical analysis of potential precursory signals

To reduce the high-frequency noise level, we calculate a moving average using time windows of 1 hour and 50 min (Fig. 2B). We find that the maximum of the moving average is the last point (the average of the stack in the 1 hour and 50 min preceding the earthquakes). Its ratio to the maximum of the stack moving average in the last 2 days (excluding the latest 1 hour and 50 min) is 1.82 (a moving median gives a slightly larger ratio of 2.1). The likelihood that the last point of the moving average is the largest by chance is less than 0.2% (*32*). The likelihood that the last point of the moving average is twice as large as the maximum on the [−48, −2]-hour time period is much smaller. The ratio between the last point of the moving average and the standard deviation of the stack moving average in the last 2 days (excluding the latest 1 hour and 50 min) provides an estimate of the signal-to-noise ratio and is equal to 3.85 (3.9 with a moving median). Moreover, we find that the last 23 points of the moving average monotonically increase and that the last 7 points exceed the maximum in the [−48, −2]-hour period. This means that these last 7 points of the moving average are larger than all values in the 48 hours before them. We perform the analysis on 100,000 random time windows of GPS data not preceding earthquakes. The last point of the moving average exceeds 1.82, and the 23 last points monotonically increase (the value found before the earthquakes) for only 0.03% of the drawn samples (*32*), providing a rough estimate of the likelihood that the signal we observe arises from noise.

S is well fitted by an exponential function of time constant τ = 1.3 hours (Fig. 2C). The misfit reduction of the fitted exponential function in

[1]Université Côte d'Azur, IRD, CNRS, Observatoire de la Côte d'Azur, Géoazur, France. [2]Institut de Physique du Globe de Paris, Université de Paris, CNRS, France.
*Corresponding author. Email: bletery@geoazur.unice.fr

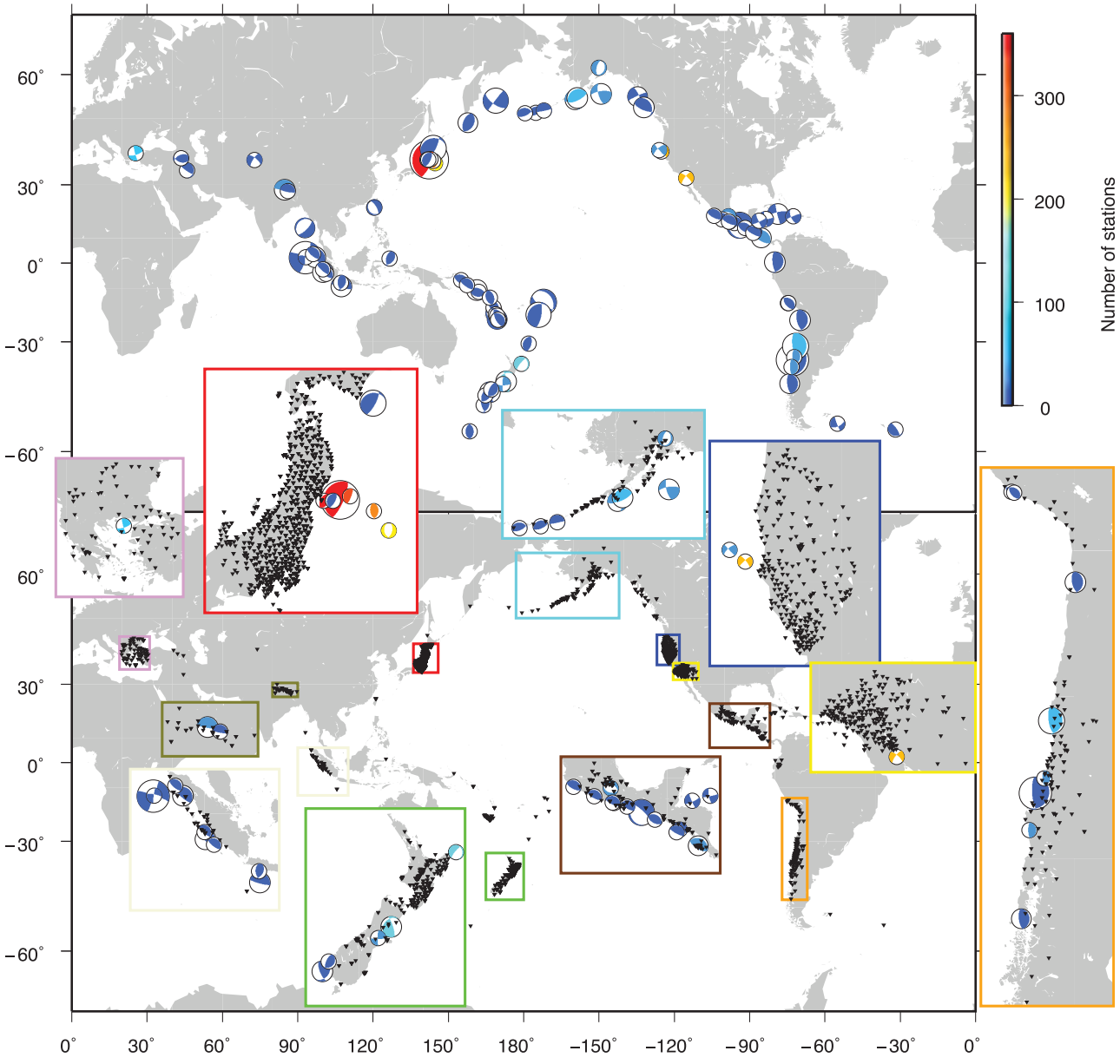

Fig. 1. Earthquakes and GPS stations used in the study. (Top) Distribution and focal mechanisms (beachball plots) of the 90 $M_w \geq 7$ earthquakes with 2 days of 5-min GPS records (with no gap and no noticeable foreshock) available within a 500-km radius of the epicenters. Mechanism sizes are indicative of event magnitudes. Colors indicate the number of time series available for each event. (Bottom) Distribution of the 3026 GPS stations with complete records in the 2 days preceding the 90 earthquakes shown above (the earthquake list is given in table S1). (Insets) Enlarged subpanels show areas of high station concentration.

the last 1 hour and 50 min is 79% (*32*), meaning that 79% of the signal in the last 1 hour and 50 min of S is explained by an exponential function. To facilitate interpretation, S can be converted into cumulative moment of preslip through a simple coefficient of proportionality (*32*). The exponential fit in moment can then be seen as a template of precursory (cumulative) moment release on the fault, suggesting that on average, earthquakes have an exponential-like precursory phase as predicted by laboratory experiments (*25*–*28*) and dynamic models (*29*–*31*). The average cumulative moment obtained before the rupture (the last point in Fig. 2C) is 3.9×10^{18} N·m, corresponding to a M_w of 6.3. Such a magnitude and duration locate precursory slip in the observation gap of fault-slip phenomena between slow aseismic slip and earthquakes (*37*). A more subtle, but noticeable, feature in S is a long-period oscillation. The best sinusoidal fit to S (Fig. 2D) gives a period of 12.9 hours, close to the period of tides (12.4 hours). However, the misfit reduction of the fitted sinusoidal function is only 10%, making the sinusoidal signal in S much less obvious than the exponential one.

To test whether the observed signals are related to fault slip in the area of the forthcoming earthquakes, we replace $\overrightarrow{g_{i,j}}$ with unit vectors pointing to arbitrary fixed directions; for simplicity, we use the east and north directions (*32*). The stack we obtain shows no signal similar to what we observe in the last 2 hours of S, nor long-period oscillation (fig. S1). This rules out that the shape of S results from a spatially correlated common-mode error in GPS data and strongly supports that the source of the signals we observed in S is related to processes taking place in the direct

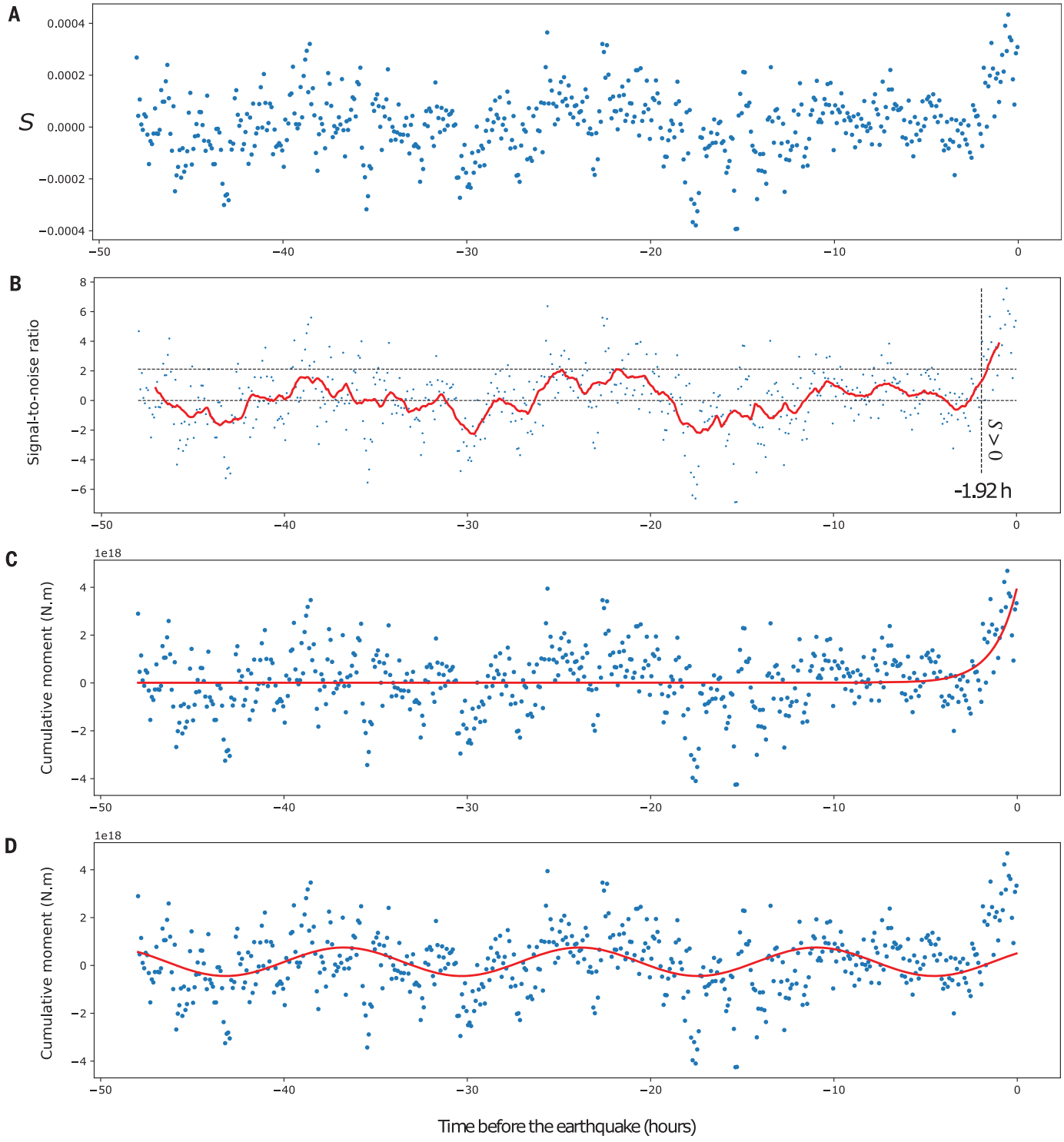

Fig. 2. Global stack in the direction of expected slip. (**A**) Global stack S of 3026 time series recorded before 90 earthquakes as a function of time relative to each earthquake origin time. (**B**) A 1-hour-and-50-min moving average of S normalized by its standard deviation on the [−48-hour, −1-hour-50-min] time period, superimposed on S. The upper horizontal dashed line indicates the maximum of the moving average (excluding the last 1 hour and 50 min). The lower horizontal dashed line indicates the 0 base line (above which observations are consistent with precursory slip). The vertical dashed line indicates the time after which the stack gives only positive values (1 hour and 55 min). The last point of the moving average is 1.82 times as large as the maximum on the [−48-hour, −1-hour-50-min] time period and 3.85 times as large as the standard deviation, providing a rough estimate of the signal-to-noise ratio. (**C**) Stack converted into moment (supplementary materials) with best exponential fit superimposed (time constant τ = 1.3 hours). (**D**) Stack in moment with best sinusoidal fit superimposed (period T = 1.9 hours).

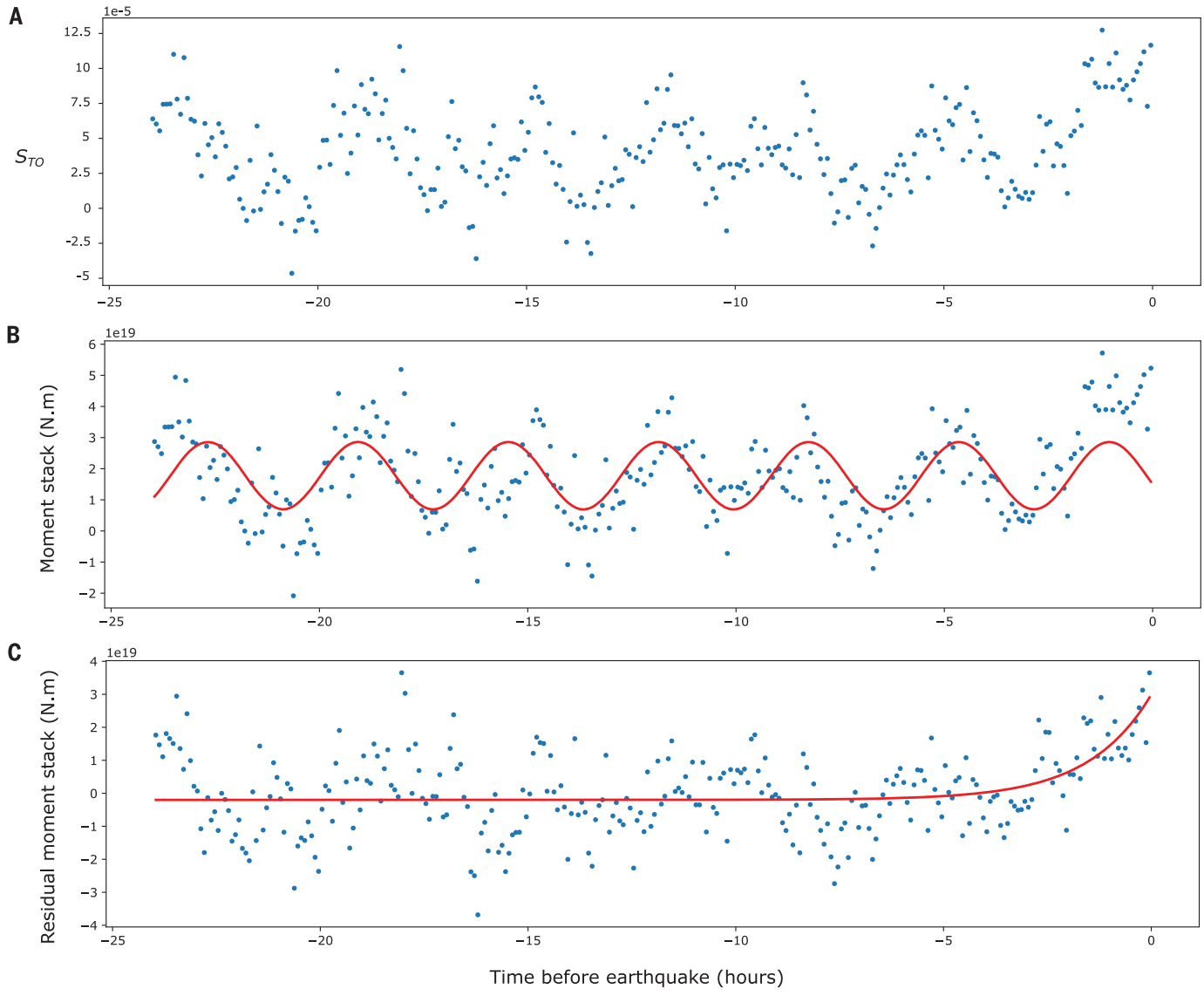

Fig. 3. Stack in the direction of expected slip for Tohoku. (**A**) Stack of 355 time series recorded before the Tohoku-Oki earthquake. (**B**) Same as (A) converted in moment release with best sinusoidal fit superimposed (period T_{TO} = 3.6 hours). (**C**) Residual of the moment-release stack with the sinusoidal fit (blue dots) and best exponential fit (red curve, time constant τ_{TO} = 1.5 hours).

vicinity of the hypocenter of the impending earthquakes.

The case of the Tohoku-Oki earthquake

The Tohoku-Oki earthquake (2011, M_w 9.0) is the largest event in our dataset. The event was also recorded by the largest number of stations (355 full time series) and is one of the few events for which short-term precursory activity was suggested by microseismicity analyses (*5*). We show the dot product stack for the Tohoku-Oki earthquake alone, S_{TO}, in the 24 hours preceding the event (Fig. 3). S_{TO} suggests precursory slip that is similar to *S*. It also reveals an unexpected but relatively clear sinusoidal shape. As for the global stack, we verify that when replacing $\overrightarrow{g_{i,j}}$ with unit vectors pointing in the east and north directions, the signal vanishes (fig. S2), strongly suggesting that this sinusoidal behavior is not related to GPS noise but rather is caused by processes taking place in the direct vicinity of the hypocenter of the Tohoku-Oki earthquake.

We find that the best fit for S_{TO} is a sinusoidal function of period T_{TO} = 3.6 hours. The misfit reduction for the 24-hour time series is 72%. We try to fit sinusoidal functions to dot product stacks calculated at 833 randomly selected 48-hour-long time windows and find 0 fit for which the misfit reduction is as high at periods below 12 hours (*32*). We also try to fit sinusoidal functions to dot product stacks calculated by changing the location of the synthetic source (*32*) and find 0 source locations that give a misfit reduction as high as for the location of the Tohoku earthquake (fig. S11A). This means that, exploring both time and space, the most periodic signal obtained in S_{TO} is found just before the event, considering a source located at the location of the hypocenter (*32*). We do not believe that sinusoidal slip has been observed on natural faults before, but similar phenomena have been observed before glacier breakoff (*38*, *39*). More precisely, glacier precursory signals are log periodic, meaning that the oscillation period decreases when getting closer to the rupture and the amplitude increases (*38*, *39*). Log-periodic precursory activity also arises from earthquake-rupture models (*40*, *41*). As for the global stack, we convert S_{TO} into moment, which can be seen as an (integrated) precursory source time function. The amplitude of the fitted sinusoid is 1.0×10^{19} N·m, corresponding

to a M_w of 6.6. This large hypothetical precursory oscillation resembles the resonance effect predicted by rate-and-state friction laws when the fault approaches its critical state (*42*). The residual of S_{TO} with the sinusoid can be fitted by an exponential of time constant T_{TO} = 1.5 hours, which is similar to the time constant of the global stack. The associated cumulative moment release is 2.9×10^{19} N·m, corresponding to a M_w of 6.9.

Contributions of individual earthquakes

Because the signal is large in S_{TO} and has a potentially large weight in S, we verify that when removing S_{TO} from the stack, the signal is still present (fig. S3). We generalize the process and evaluate the relative contribution of each earthquake in the signal observed in the last 2 hours and in the overall stack (*32*). We find that the signal is not overly dominated by one or a few earthquakes even though we see larger contributions from earthquakes recorded by many stations and by stations located close to the source of the impending earthquakes (fig. S4). In details, 52 earthquakes (58% of the total) contribute positively to the global stack during the last 2 hours, but these 52 earthquakes represent 2235 time series (74% of the time series) (*32*). Additionally, we calculate the average of the last 2 hours for the stacks on all earthquakes and find very similar figures: Fifty-four earthquakes (60%) have a positive mean in the last 2 hours of the stack, but these 54 earthquakes represent 2251 time series (74% of the total).

Discussion

Because the exponential function is always positive and monotonically increasing, a potential exponential acceleration of slip in the direction of the upcoming coseismic slip would sum constructively, making it likely to appear in the global stack. To the contrary, the oscillation properties of the sinusoidal function make a potential sinusoidal preslip unlikely to appear in a multiearthquake stack. Nonetheless, the global stack exhibits a weak sinusoidal signal. Even though the misfit reduction provided by the sinusoidal fit is only 10%, the best-fitting function has two interesting properties: (i) Its period (12.9 hours) is very close to the period of tides (12.4 hours), and (ii) its value at the earthquake origin time is close to its maximum (Fig. 2D). These two properties can potentially explain how stacked oscillations could interfere positively: A common excitation source could result in a common excited period, and an earthquake triggering at the most favorable time could explain the absence of phase lag. Correlations have been observed between tides and microseismicity (*43*, *44*), suggesting tidal modulation of slow aseismic slip (*45*, *46*). Correlations between tides and earthquakes have also been observed in time periods preceding large earthquakes, suggesting that when the faults are approaching the critical stage of failure, tidal loading may initiate a rupture (*47*, *48*). A 12-hour oscillation on the faults in the days preceding the events is therefore physically consistent with a tidal excitation of the system, possibly enhanced by a resonance effect (*42*), as the faults reach their critical state.

Conclusions

Our analysis indicates that, on average, earthquakes start with a ≈2-hour-long exponential-like acceleration of slow slip. Analysis of foreshock activity also suggests exponential acceleration of fault slip but over a much wider range of timescales (*7*). The observation we make on GPS time series might be the very end of much a longer process of precursory slip. Although present instrumental capacities do not allow us to identify precursory slip at the scale of individual earthquakes, our observation suggests that precursory signals exist and that the precision required to monitor them is not orders of magnitudes away from our present capabilities.

REFERENCES AND NOTES

1. C. H. Scholz, L. R. Sykes, Y. P. Aggarwal, *Science* **181**, 803–810 (1973).
2. Y. Y. Kagan, *Geophys. J. Int.* **131**, 505–525 (1997).
3. R. J. Geller, *Geophys. J. Int.* **131**, 425–450 (1997).
4. M. Bouchon *et al*., *Science* **331**, 877–880 (2011).
5. A. Kato *et al*., *Science* **335**, 705–708 (2012).
6. S. Ruiz *et al*., *Science* **345**, 1165–1169 (2014).
7. M. Bouchon, V. Durand, D. Marsan, H. Karabulut, J. Schmittbuhl, *Nat. Geosci.* **6**, 299–302 (2013).
8. B. Schurr *et al*., *Nature* **512**, 299–302 (2014).
9. M. Bouchon *et al*., *Nat. Geosci.* **9**, 380–383 (2016).
10. M. Radiguet *et al*., *Nat. Geosci.* **9**, 829–833 (2016).
11. J. R. Bedford *et al*., *Nature* **580**, 628–635 (2020).
12. A. Socquet *et al*., *Geophys. Res. Lett.* **44**, 4046–4053 (2017).
13. A. P. Mavrommatis, P. Segall, K. M. Johnson, *Geophys. Res. Lett.* **41**, 4486–4494 (2014).
14. E. E. Brodsky, T. Lay, *Science* **344**, 700–702 (2014).
15. S. Ruiz, *et al*., *Geophys. Res. Lett.* **44**, 10290–10297 (2017).
16. W. L. Ellsworth, F. Bulut, *Nat. Geosci.* **11**, 531–535 (2018).
17. C. Tape *et al*., *Nat. Geosci.* **11**, 536–541 (2018).
18. E. Caballero *et al*., *Geophys. Res. Lett.* **48**, GL091916 (2021).
19. S. Y. Schwartz, J. M. Rokosky, *Rev. Geophys.* **45**, RG3004 (2007).
20. J. Gomberg, Cascasdia 2007 and Beyond Working Group, *Geol. Soc. Am. Bull.* **122**, 963–978 (2010).
21. K. Obara, A. Kato, *Science* **353**, 253–257 (2016).
22. Q. Bletery, J.-M. Nocquet, *Nat. Commun.* **11**, 2159 (2020).
23. L. M. Wallace, *Annu. Rev. Earth Planet. Sci.* **48**, 175–203 (2020).
24. W. M. Behr, R. Bürgmann, *Philos. Trans. R. Soc. London Ser. A* **379**, 20200218 (2021).
25. M. Ohnaka, L. Shen, *J. Geophys. Res.* **104**, 817–844 (1999).
26. S. Latour, A. Schubnel, S. Nielsen, R. Madariaga, S. Vinciguerra, *Geophys. Res. Lett.* **40**, 5064–5069 (2013).
27. F. X. Passelègue *et al*., in *Fault Zone Dynamic Processes: Evolution of Fault Properties during Seismic Rupture*, M. Y. Thomas, T. M. Mitchell, H. S. Bhat, Eds. (Wiley, 2017), pp. 229–242.
28. C. Hulbert *et al*., *Nat. Geosci.* **12**, 69–74 (2019).
29. J. H. Dieterich, B. Kilgore, *Proc. Natl. Acad. Sci. U.S.A.* **93**, 3787–3794 (1996).
30. A. M. Rubin, J.-P. Ampuero, *J. Geophys. Res. Solid Earth* **110**, B11312 (2005).
31. Y. Kaneko, S. B. Nielsen, B. M. Carpenter, *J. Geophys. Res. Solid Earth* **121**, 6071–6091 (2016).
32. Materials and methods are available as supplementary materials.
33. G. Blewitt, W. C. Hammond, C. Kreemer, *Eos* **99**, 485 (2018).
34. T. R. Stevenson, *Phys. Rev. D Part. Fields* **56**, 564–587 (1997).
35. Y. Tyapkin, B. Ursin, *J. Geophys. Eng.* **2**, 177–187 (2005).
36. J.-P. Montagner *et al*., *Nat. Commun.* **7**, 13349 (2016).
37. S. Ide, G. C. Beroza, D. R. Shelly, T. Uchide, *Nature* **447**, 76–79 (2007).
38. J. Faillettaz, A. Pralong, M. Funk, N. Deichmann, *J. Glaciol.* **54**, 725–737 (2008).
39. J. Faillettaz, M. Funk, C. Vincent, *Rev. Geophys.* **53**, 203–224 (2015).
40. D. Sornette, C. G. Sammis, *J. Phys. I* **5**, 607–619 (1995).
41. R. C. Viesca, *Phys. Rev. E* **93**, 060202 (2016).
42. H. Perfettini, J. Schmittbuhl, J. R. Rice, M. Cocco, *J. Geophys. Res.* **106**, 13455–13472 (2001).
43. J. L. Rubinstein, M. La Rocca, J. E. Vidale, K. C. Creager, A. G. Wech, *Science* **319**, 186–189 (2008).
44. A. M. Thomas, R. M. Nadeau, R. Bürgmann, *Nature* **462**, 1048–1051 (2009).
45. J. C. Hawthorne, A. M. Rubin, *J. Geophys. Res. Solid Earth* **115**, B09406 (2010).
46. H. Houston, *Nat. Geosci.* **8**, 409–415 (2015).
47. S. Tanaka, *Geophys. Res. Lett.* **37**, L02301 (2010).
48. S. Tanaka, *Geophys. Res. Lett.* **39**, L00G26 (2012).
49. Q. Bletery, J.-M. Nocquet, Scripts to reproduce the results of "The precursory phase of large earthquakes" (Science, 2023), Zenodo (2023); https://doi.org/10.5281/zenodo.8064086.
50. Nevada Geodetic Laboratory (2023); geodesy.unr.edu.

ACKNOWLEDGMENTS

We are grateful to J.-P. Ampuero, G. Nolet, G. Blewitt, J.-P. Avouac, D. Rivet, C. Twardzik, and F. Passelègue for helpful discussion. **Funding:** This project has received funding from the European Research Council (ERC) under the European Union's Horizon 2020 research and innovation program (grant agreement 949221) and from the French National Research Agency (grant agreement ANR-19-CE310003). **Author contributions:** Q.B. had the original idea. J.-M.N. provided numerical tools (PYACS python library) and expertise on GNSS data. Both authors contributed to the analysis, interpretation, and preparation of the manuscript. **Competing interests:** The authors declare that they have no competing interests. **Data and materials availability:** All the scripts and data used to perform this study are available at Zenodo (*49*). The PYACS library we used for data processing and Green's functions calculation is available at github.com/JMNocquet/pyacs36. The GPS time series we used are available on the website of the Nevada Geodetic Laboratory of the University of Nevada Reno (*50*).

SUPPLEMENTARY MATERIALS

science.org/doi/10.1126/science.adg2565
Materials and Methods
Figs. S1 to S11
Table S1
References (*51*–*53*)

Submitted 12 December 2022; accepted 17 May 2023
10.1126/science.adg2565

The precursory phase of large earthquakes

Quentin Bletery and Jean-Mathieu Nocquet

Science, **381** (6655), .
DOI: 10.1126/science.adg2565

Editor's summary
Unlike some volcanic eruptions, no clear set of precursor signals have been identified for large earthquakes. Bletery and Nocquet analyzed high-rate GPS time series before 90 different earthquakes that were magnitude 7 and above to find a precursor signal (see the Perspective by Bürgmann). They observed a subtle signal that rose from the noise about 2 hours before these major earthquakes occurred. This work may allow fault monitoring for this precursor phase with denser and higher-precision instrumentation. —Brent Grocholski